12th International Symposium on Turbulence and Shear Flow Phenomena (TSFP12)
Osaka, Japan (Online), July 19-22, 2022

VORTICAL STRUCTURES IN THE INITIAL REGION OF A ROUND JET WITH BIFURCATING FLOWS

Akinori Muramatsu
Department of Aerospace Engineering,
College of Science and Technology,
Nihon University
7-24-1 Narashinodai, Funabashi, Chiba, 274-8501, Japan
muramatsu.akinori@nihon-u.ac.jp

Kohei Tanaka
Major of Aerospace Engineering,
Graduate School of Science and Technology,
Nihon University
7-24-1 Narashinodai, Funabashi, Chiba, 274-8501, Japan
csko19017@g.nihon-u.ac.jp

ABSTRACT

The formation of a side jet in the initial region of a round jet is concerned with the wavy deformation of a vortex ring and a pair of streamwise vortices. These phenomena are difficult to investigate to be unstable, and the details are not clear. Therefore, this study aims to clarify the formation mechanism of side jets. To achieve this, we fixed the forming positions of the side jets by controlling both the wavy deformation of the vortex ring and the formation of streamwise vortices, using synthetic jets installed in a round nozzle. The following became clear from the controlled experiment and its numerical simulation. The side jets occur due to the secondary instability that develops in the braid region. The side jet is the flow induced outwardly in the radial direction by the circulations of a vortex ring and a pair of streamwise vortices. The apparently continuous flow of a side jet results from the periodic repetition of induced flow between vortex rings and the streamwise vortices.

INTRODUCTION

Bifurcating flows are formed at the initial region of a jet, when the mass density of jet fluid is lower than that of ambient fluid. Monkewitz et al. (1990) observed the bifurcating flows in a round heated air jet, and Kyle and Sreenivasan (1993) found them in a round jet with helium gas and air mixture. The bifurcating flows are called side jets. The side jet is easily observed in a low density jet. However, Muramatsu, A. et al. (2015) found that the side jet is also formed in a uniform mass density jet. The formation of side jets in a round jet with uniform mass density has been suggested using a numerical simulation by Brancher et al. (1993). When the side jets are formed in a round jet, velocity fluctuation in the potential core is relatively high and periodic, so that vortex rings are periodically formed and deformed wavy at the downstream (Monkewitz et al, 1990; Kyle and Sreenivasan, 1993; Muramatsu et al., 2008). The generation of the high and periodic velocity-fluctuation is concerned with the velocity gradient of a jet flow at the nozzle exit, and the side jets are formed in the certain range of the velocity gradient (Kyle and Sreenivasan, 1993; Kato and Muramatsu, 2017). Moreover, it is thought that streamwise vortex is related to the wavy deformation of a vortex ring (Toyoda et al., 1999).

Various mechanisms for the side-jets formation have been proposed. For the case of a low density jet, it is considered that the vorticity of a lateral vortex or vortex ring is enhanced by the baroclinic torque (Chassaing et al., 2002). Brancher et al. (1993) indicate that a side jet is a flow induced by a pair of streamwise vortices with different rotational directions formed in the braid region. However, the details of mechanism for the side-jets formation have not been well understood. The reason is that the position of the side-jet formation changes irregularly and it is difficult to measure the flow involved the side jet. That is, since the starting position of the side jet rotates irregularly, it is particularly difficult to measure the streamewise vortices in the initial region of a jet.

We have considered that an experiment is conducted by suppressing the azimuthal rotation of the side-jets, namely the azimuthal rotation of a vortex ring formed in the jet shear layer (Muramatsu and Tanaka, 2021). Three synthetic jets are located in the nozzle, and give the jet periodic disturbances, so that the azimuthal rotation of the vortex ring is stopped and the formation positions of the side jets are fixed. In this condition, since the side jets change from an irregular phenomenon to a periodic phenomenon, it is possible to process the measured data by synchronizing with the phase. Vortical structures for the side-jet formation were determined using a time-resolved PIV and 3D-imaging with Mie scattering (Kawabe et al., 2014). In the adition, a numerical simulation of a round jet with bifurcating flows was performed by simulating the experimental equipment used here, using an open-source software OpenFOAM, so that details of vortical structure were obtained in the jet with bifurcations.

EXPERIMENTAL APPARATUS AND METHODS

Experimental Apparatus

Figure 1 shows a schematics diagram of a round contraction nozzle with three holes for acoustic excitation. The outlet diameter of the round nozzle is D_0 = 12 mm and the area contraction ratio is 30.3. A cylindrical actuator equipped with three holes with a diameter d_0 of 2 mm is attached to the top of the round nozzle, as shown in Fig. 1. The height of the actuator is 12 mm. The periodic disturbance added to the jet is generated using loudspeakers. The loudspeaker is sinusoidally vibrated in the speaker box, and the vibration propagates through a vinyl tube to the excitation holes and forms synthetic jets at the excitation holes.

A downstream view of the nozzle is shown in Fig. 2. The nozzle has three holes at azimuthally equal intervals. Three synthetic jets are used to excite the jet at equal phases from the outside in the radial direction toward the center.

The coordinate system has the origin at the center of the nozzle outlet, with x in the mainstream direction, y in the lateral direction, and z in the depth direction, as shown in the left diagram of Fig. 2.

Experimental Conditions

Experimental conditions are shown in Table 1. Air is ejected

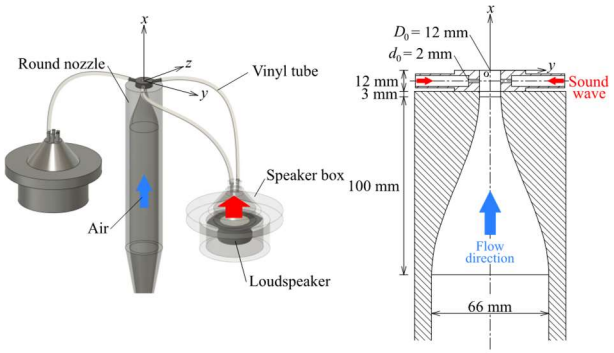

Figure 1. Round nozzle with small holes to add disturbances to the jet in the nozzle.

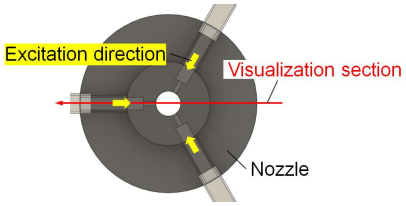

Figure 2. Excitation directions and visualized section.

vertically upward from the round nozzle into the ambient air. The Reynolds number Re of the jet is set to be 2,000. The issuing velocity U_{c0} under this condition is 2.55 m/s at the nozzle exit on the centerline, as the Re is defined by the U_{c0} and D_0. The formation frequency of vortex rings of the round jet in the natural transition at Re = 2,000 is 120 Hz. This value was determined by flow visualization and velocity measurement using a hot wire anemometer. Therefore, the input signal to the loudspeaker is a sine wave with a frequency of f_s = 120 Hz. The nondimensional frequency $St = f_s D_0/U_{c0}$ is 0.565. The velocity in the flow direction of the synthetic jet changes periodically from -0.4 to 0.5 m/s, and the turbulence intensity is approximately 10%

Experimental Methods

The jet cross-section was visualized using a laser sheet with a thickness of 1 mm. Fine particles with a nominal diameter of 1 μm generated by a smoke generator were mixed with the jet fluid and then the air jet issued into the still atmosphere from the nozzle. A high-speed camera was used to capture cross-sections in the streamwise direction (position is shown in Fig. 2) and the horizontal sections perpendicular to the mainstream.

For a PIV measurement, it is necessary to mix particles in the surrounding air. Therefore, a duct was installed around the nozzle, and the inside of the duct was filled with particles. Images for time-resolved PIV were recorded using a high-speed camera at 12,500 fps with a resolution of 1,024 × 1,024 pixels. Velocity fields were obtained from the images using a PIV analysis software with an overlap of 50% and an nterrogation window of 32 × 32 pixels.

In the addition, an oscillating mirror method was adopted for a time-resolved 3D imaging. The laser sheet was scanned at high speed by the oscillating the mirror. Several cross-sectional images were taken with a high-speed camera almost simultaneously, and three-dimensional images were constructed by stacking these images.

Table 1. Experimental conditions.

Jet gas	Air
Jet Reynolds number, Re	2,000
Nozzle diameter, D_0 [mm]	12
Issuing velocity, U_{c0} [m/s]	2.55
Frequency for generation of vortex rings, f_v [Hz]	120
Non-dimensional frequency, St	0.565
Input signal to loudspeaker	Sine wave
Frequency of input signal, f_s [Hz]	120
Turbulence intensity, u'/U_{c0} [-]	0.10

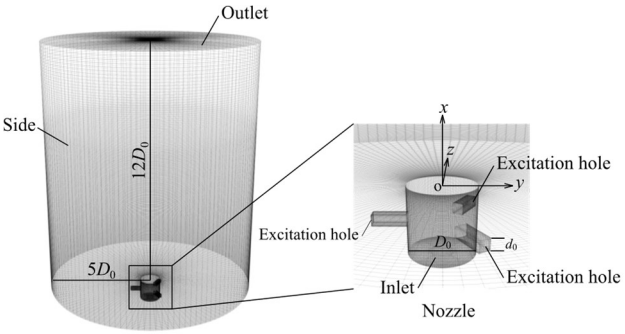

Figure 3. Computational domain.

SETUP FOR NUMERICAL SIMULATION

Computational Domain and Elements

Figure 3 shows a computational domain. The computational domain consists of the cylindrical part of the nozzle with the excitation holes and the main computational domain (space ejected from the nozzle). The sizes of the main computational domain are $5D_0$ in the radial direction, 2π in the azimuthal direction, and 12 D_0 in the mainstream direction. The computational elements are made smaller from the center of the nozzle toward the shear layer and larger from the shear layer toward the lateral boundary, and they are made smaller near the nozzle exit in the mainstream direction. The computational elements are made in a cylindrical coordinate system outside the radial direction from the Cartesian coordinate system near the center of the nozzle.

The nozzle at the bottom of the main computational domain is cylindrical with a diameter of 12 mm (D_0) and a height of 12 mm, and the experimental actuator is reproduced. The excitation holes are a cylinder with a diameter of 2 mm (d_0) in the experiment, but in the calculation, they are rectangular with a side of 2 mm, and three holes are provided at equal intervals in the azimuthal direction.

Boundary and Initial Conditions

As the velocity inflow boundary condition, a velocity profile in the mainstream direction flowing into the computational domain from the bottom of the cylindrical nozzle (inlet in Fig. 3) gives a Top-Hat type velocity profile as expressed by the following equation (1).

$$U_x(r,t) = \frac{1}{2}U_c^{\text{inlet}}\{1 + U^{\text{noise}}(r,t)\}\left[1 - \tanh\left\{a\left(\frac{r}{D_0} - r_0\right)\right\}\right] \quad (1)$$

Here, $r = \sqrt{y^2 + z^2}$, and two constants a and r_0 are a = 30 and r_0 = 0.45 on the based the measured velocity profile using a hot wire anemometer. To set the Re of the issuing air to 2,000, the U_c^{inlet} is 2.5 m/s. For the velocity U_x in the mainstream direction, a spatially and temporally random disturbance U^{noise} with ± 0.5% of the U_c^{inlet} is added as a disturbance simulating white noise.

The disturbances caused by the periodic vibration of the loudspeaker are reproduced under the pressure boundary condition at the excitation hole, and the boundary condition is given by the following equation (2).

$$p/\rho = A\sin(2\pi f_s t) \quad (2)$$

The amplitude A is adjusted so that the turbulence intencity is close to the experimental value, and the A is chosen to be 2.0 m^2/s^2. The frequency f_s is set to 120 Hz and the same as the sinusoidal input signal to the loudspeakers.

The boundary conditions of the side and outlet in Fig. 3 are constant total pressure and take into account the inflow and outflow. The area corresponding to the wall surface in Fig. 3 (the bottom surface excluding the cylindrical nozzle in the main computational domain and the inner wall of the cylindrical nozzle) adopts a non-slip condition.

Initial conditions are set to 0 for velocity $\boldsymbol{U}$ [m/s] and pressure divided by density p/ρ [m^2/s^2] in all regions except the boundaries expressing in Eqs. (1) and (2).

Computational Methods

The governing equations are the continuity equation and the Navier-Stokes equation for an incompressible fluid. A numerical simulation was performed using an open source software OpenFOAM under the same conditions as in the above experiment. We used the pimpleFoam solver for uncompressible and unsteady flows. The solver discretizes the governing equations using the finite volume method and calculates velocity and pressure using the PISO (Pressure Implicit with Splitting of Operators) method. The turbulence models are not used, that is an implicit LES. The calculation time interval is adjusted for each calculating step so that the maximum Courant number does not exceed 0.5. The time integration is an implicit Euler method.

RESULTS AND DISCUSSION

Flow Visualizations by a Planar Laser Mie Scattering

Figure 4 shows visualized images of an x-y cross-section of the excited jet in the streamwise direction. Figure 4(a) shows an instantaneous image, and Fig. 4(b) is a phase-averaged image at the same phase as Fig. 4(a) based on the phase of the exciting frequency. A white arrow at the bottom in Fig. 4 indicates the exciting direction. The periodic excitation from the radial direction brings the formation position of a vortex ring closer to the nozzle exit than that of the jet of natural transition. In addition, the collapse position of the vortex ring is also on the upstream side, and a series of phenomena from the formation to the collapse of the vortex ring is enhanced (Muramatsu and Tanaka, 2021). A side jet branching radially outward near x/D_0 = 2.0 are formed on the unexcited side. As shown by red lines in Fig. 4, the vortex ring precedes on the side where the side jet is formed. This excited side jet is considered to be a bifurcating

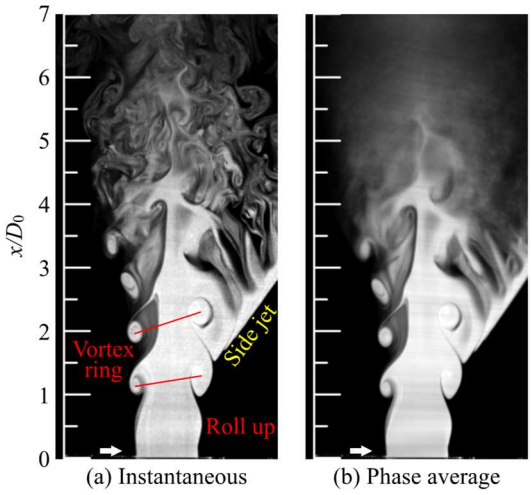

Figure 4. Visualized streamwise cross-sections of a excited air jet.

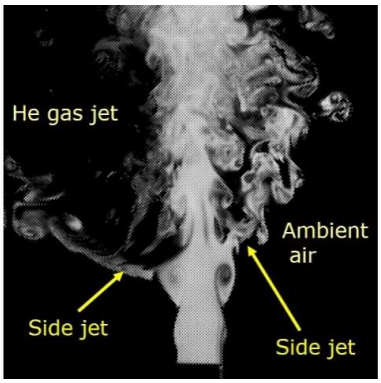

Figure 5. Visualized streamwise cross-sections on the centerline of a round helium gas jet at Re = 1,000.

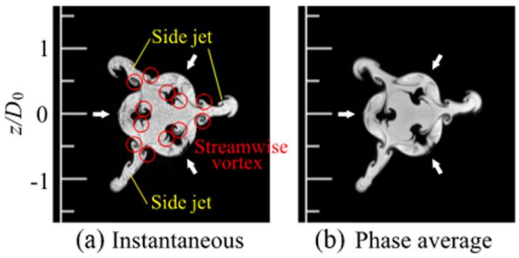

Figure 6. Visualized horizontal cross-sections of a excited air jet at x/D_0 = 2.0.

flow by the same mechanism as side jets in a helium gas jet shown in Fig. 5.

Figure 6 shows the visualized images of the horizontal cross section (y-z cross section) at x/D_0 = 2.0. Figures 6 (a) and (b) are respectively an instantaneous image and phase average image. Figure 6 has the same phase as that of Fig 4. As seen in Fig. 4, the images of the horizontal cross section at x/D_0 = 2.0 are the phase of a vortex ring when the jet passes the cross section. The excitation changes the shape of the y-z cross section of the jet to a triangle. The vortical structures inside and outside the vortex ring shown in red circles in Fig. 6(a) are pairs of streamwise

vortices with streamwise vorticity, as will be shown later in the results by PIV measurements. It can be observed that the two counter-rotating streamwise vortices are paired, and a side jet is formed between a pair of streamwise vortices.

Because the phase-averaged images in Fig. 4(b) and 6(b) clearly show the structures of the potential core, vortex rings, streamwise vortices, and side jet until the vortex ring collapses, it is indicated that these structures are a flow locked-in at the exciting frequency. Therefore, these structures can be treated as the aimed periodic phenomenon.

Focusing on the deformation of the vortex ring, it is considered that the vortex ring is three-dimensionally wavy because it is deformed in the streamwise direction in Fig. 6 and in the azimuthal direction in Fig. 7.

Visualizations of Vortical Structures in the Horizontal Plane by PIV Measurement

To visualize the vortical structures in the horizontal cross section (y-z cross section) more clearly, the streamwise vorticity ω_x was obtained from the measured results by a PIV and is shown as a contour diagram in Fig. 7. The contour diagrams are dimensionless by the maximum vorticity in each cross-section, and the positive values are counterclockwise. Figure 7(a) and (b) respectively show the cross sections at $x/D_0 = 1.5$ and $x/D_0 = 2.0$, and they are in phase. The flow structures indicated by the red circles in Fig. 6 are streamwise vortices, because they have vorticities ω_x as indicated by the circles in Fig. 7(b).

The vorticity of the streamwise vortex can be seen at six locations in Fig. 7(a). Since the jet is excited from three locations, two streamwise vortices are formed for each excited hole. On the other hand, in Fig. 7(b), streamwise vortices can be seen at 12 locations, which is twice as many as in Fig. 7(a). It can also be seen that the outgoing flows are generated between the streamwise vortex pairs.

Next, we focus on the y-z cross section in the vortex ring at $x/D_0 = 2.0$ shown in Fig. 8. In this y-z cross section, there are six regions where the absolute value of the streamwise vorticity ω_x is larger than that of the streamwise vortices, as indicated by the circles in Fig. 8. Comparison with the visualized image in Fig. 6 shows that the vorticities are expressed in the cross-section of the vortex ring. If the vortex ring is not deformed in the streamwise direction, the vorticity ω_x does not appear in the horizontal cross-section (y-z cross-section). However, if the vortex ring is deformed in three dimensions as described previously, the vorticities are measured as shown in the schematic diagram in Fig. 9. When the vortex ring is three-dimensionally deformed as shown in a yellow ring in Fig. 9 and flows downstream while rotating, the vorticities rotating in the red and blue directions are measured in the plane as the vortex ring passes through the measurement plane. The numbers in Fig. 9 correspond to the numbers assigned to the vorticity in Fig. 8, and the red and blue arrows represent the vorticity that appears when the vortex ring rotating in the poloidal direction passes through the plane. It can also be seen that the outflows are generated at the upper part of the mountainous part of the wavy deformed vortex ring from Figs. 8 and 9.

3D Image of a Jet with Bifurcating Flows

The spatial distribution of the wavy deformed vortex ring shown in Fig. 9 and the streamwise vortices shown in Fig. 7 is revealed from the three-dimensional imaging of the jet shown in Fig. 10. As shown in Fig. 9, the vortex ring is greatly deformed

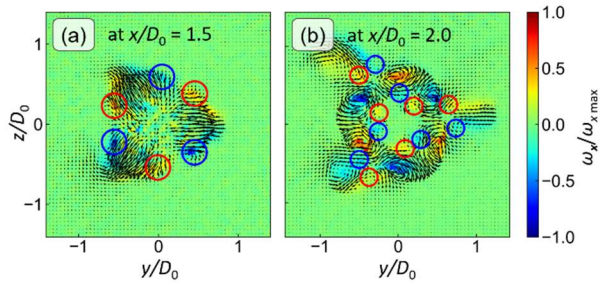

Figure 7. The streamwise vorticity field in the horizontal cross sections.

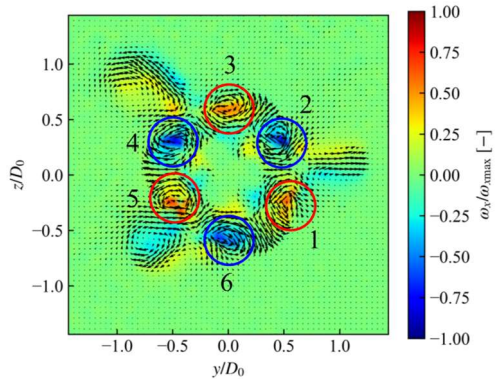

Figure 8. The streamwise vorticity field in the horizontal cross section at $x/D_0 = 2.0$.

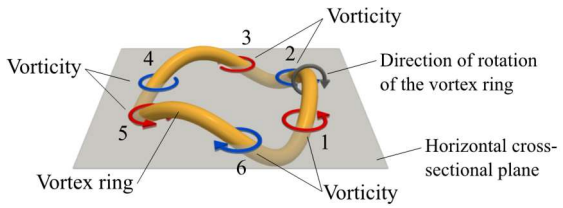

Figure 9. Wavy deformation of a vortex ring.

in a wavy shape, and a pair of streamwise vortices can be seen around the vortex ring. The streamwise vortices extend from the outside of the upstream vortex ring to wrap around the inside of the downstream vortex ring.

Figure 11 is a schematic diagram of the vortical structures inferred from the three-dimensional imaging of Fig. 10. The side jets are formed between the upper side of mountains of the poloidally rotating vortex rings and the streamwise vortex pairs that develop in the braid region.

Visualizations of Vortical Structures by Numerical Simulation

Figure 12 shows the round air jet with bifurcating flows, namely side jets, by a numerical simulation. Based on the calculated velocity field, the jet is visualized with particles ejected from the nozzle. This visualization allows us to confirm the vortex rings and side jets. Since the stripe pattern between the side jets and the mainstream that appears in the cross-sectional image in Fig. 4 also is observed in Fig. 12, it is judged that the reproducibility of the flow field by calculation is high.

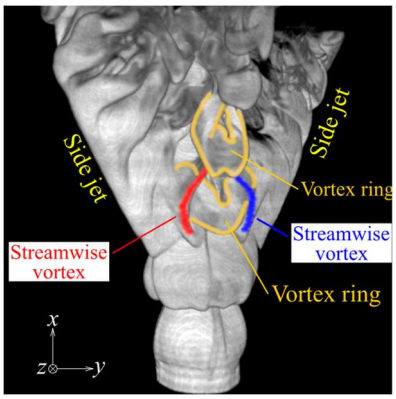

Figure 10. 3D image of the jet with side jets.

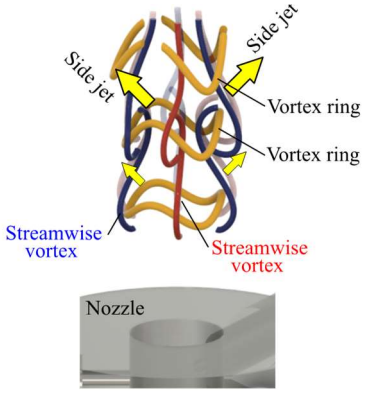

Figure 11. A schematic diagram of the vortical structures.

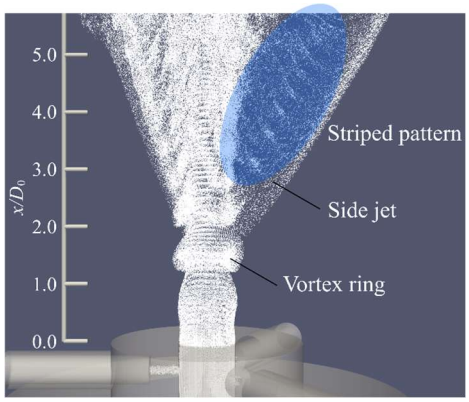

Figure 12. Visualization of flow field obtained by numerical simulation with tracer particles.

Although the results are not shown here, the values of the mean velocity and turbulence intensity are also close to the measured values by our experiment.

From the numerical simulation result, vortical structures are extracted using the Δ value (Chong et al., 1990) to investigate coherent structures such as vortex rings and streamwise vortices, and to consider the structure of the flow field. The vortical structures identified by the isosurface of the Δ value strongly depends on the threshold value. Figure 13 shows the difference in vortical structures depending on the threshold value. The color

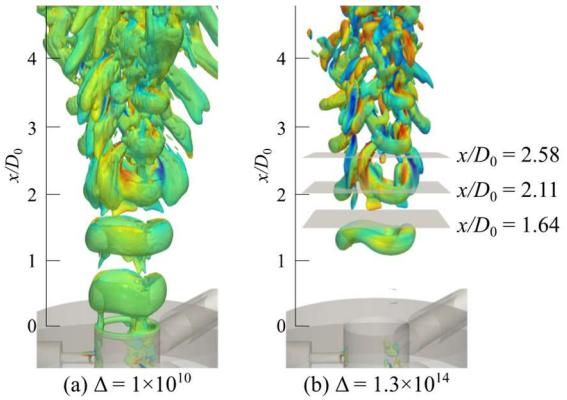

Figure 13. Comparison of extracted vortical structures by threshold values of Δ.

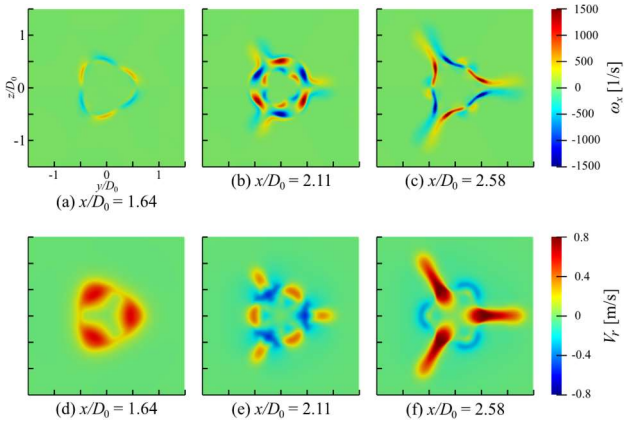

Figure 14. Streamwise vorticity fields (upper) and radial velocity fields (lower) in horizontal sections.

coding in Fig. 13 corresponds to the positive (red) to and negative (blue) values of ω_x as similar in Figs. 7 and 8. Figure 13(a) shows the case where the threshold value is set such that the roll-up of the shear layer seen in Fig. 4 is identified as a vortex, and Fig. 13(b) shows the case where the threshold value is set such that the roll-up is not identified as a vortex. Figure 13 (a) also captures the deformation of the shear layer due to excitations in the nozzle. The deformation of the shear layer is located below the first vortex ring, and the vortex ring is accompanied the deformation of the shear layer caused by disturbances caused in the nozzle. However, Fig. 13(a) is difficult to capture the relationship between the vortex ring and the streamwise vortices, so in the subsequent discussion, the threshold is set as shown in Fig. 13(b).

Secondary Instability

Figure 14 shows the streamwise vorticity ω_x and radial velocity V_r in three horizontal cross sections (y-z cross sections) to consider the relationship between the growth of streamwise vortices and the formation of side jets. The locations of the three cross sections are the braid regions (x/D_0 = 1.64 and 2.58) and the vortex ring region (x/D_0 = 2.11), as shown in Fig. 13(b). Disturbances due to excitation appear as strains in the shear layer, and the strains are induced streamwise vorticities in the braid region (Fig. 13(a)), causing in in-plane flows (Fig. 13(d)). The

streamwise vorticities are sufficiently developed by elongation in the deformed vortex ring region (Fig. 13(b)). Three pairs of streamwise vortices are formed in this process, and it can be confirmed that the streamwise vortices extend from the inside of the downstream vortex ring to the outside of this vortex ring from the isosurface of Δ in Fig. 12 (b).

It can be seen that the in-plane circulations that occur as a result of the development of the streamwise vorticities in the braid region induces radial velocities between streamwise vortex pairs from Figs. 13(c) and 13(f). These radial outward flows occur uninterruptedly from the center of the jet to the periphery in the braid region (Fig. 13(f)). On the other hand, the outflows are divided by the flow toward the center in the vortex ring region (Fig. 13(e)). Therefore, the side jets are considered to be the phenomenon by the secondary instability that develops in the braid region.

Interference of Vortex Ring and Streamwise Vortices and Formation of Side Jet

Figure 15 shows vortical structures by the isosurface of the Δ value in time series. The contours of the radial velocity are superimposed on the right side in Fig. 15. The data were extracted within one cycle $T = 1/f_s$ based on the exciting frequency f_s. It can be seen that the streamwise vortices grow upstream from the inside of the second vortex ring in Fig. 15 (a) to the outside of the second vortex ring in Fig. 15 (c). That is, the streamwise vortices extending from the inside of the downstream vortex ring are connected to the vortex ring so as to wrap around the outside of the upstream vortex ring. In this way, the development of the streamwise vortices is accompanied by the wavy deformation of the upstream vortex ring, and the interference between the vortex ring and the streamwise vortices is periodically repeated. However, this result on the interference between the vortex rings and streamwise vortices seems to differ from the previous result (Toyoda et al., 1999) that streamwise vortices form in a hairpin shape. It can be seen that the disturbances are propagated from the downstream to the upstream by the streamwise vortices. Therefore, it is considered that the streamwise vortices cause local absolute instability (Monkewitz and Sohn, 1988; Muramatsu and Hara, 2016), so that large velocity fluctuations due to a self-excited oscillation produce in the potential core.

CONCLUSIONS

The formation mechanism of side jets in the initial region of a round jet was investigated using a round air jet with an artificially formed bifurcating flows and the following findings were obtained. Side jets are formed as a result of secondary instability that develop in the braid region. A side jet is formed between the upper part of the mountain part of a three-dimensionally wavy vortex ring and a pair of the streamwise vortices in the blade region. The side jet is the flow induced radially outward in the region between the poloidal circulation of the vortex ring and the circulation of the streamwise vortex pair. The streamwise vortex pair extends from the downstream vortex ring to the upstream vortex ring, and it is thought that disturbances are transmitted to the downstream by the streamwise vortex pair and they cause absolute instability. The formation of side jets is a periodic phenomenon linked to the roll-up of shear layer, namely the formation of a vortex ring. The apparently continuous flows of the side jets are the result of periodically repeated interference between the wavy deformation of the vortex ring and the streamwise vortices.

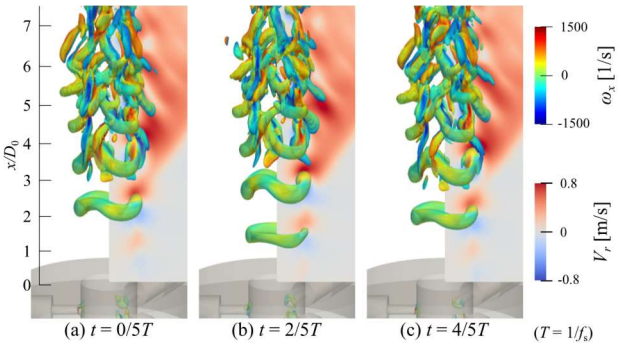

Figure 15. Periodic changes in vortical structures.

REFERENCES

Brancher, P., Chomaz, J. M., and Huerre, P., 1993, "Direct numerical simulations of round jets: Vortex induction and side jets," *Physics of Fluids*, Vol. 6, pp. 1768-1774.

Chassaing, P., Antonia, R. A., Anselmet, F., Joly, L., and Sarkar, S., 2002, "*Variable density fluid turbulence*," Vol. 69 of *Fluid mechanics and its applications*. Kluwer Academic Publishers, Chap. 8.

Chong, M. S., Perry, A. E. and Cantwell, B. J., 1990, "A general classification of three-dimensional flow fields," *Physics of Fluids*, Vol. 2, No. 5, pp. 765-777.

Kato, Y. and Muramatsu, A., 2017, "Effect of initial velocity gradient on side-jets formation in a round jet with constant density," *Extend Abstract of the Ninth JSME-KSME Thermal and Fluid Engineering,* TFEC9-1311.

Kawabe, K., Harada, H., and Muramatsu, A., 2014, "Three-dimensional imaging of a helium gas jet flow using planer laser Mie scattering," *Proceedings of the 16th International Symposium on Flow Visualization*.

Kyle, D. M. and Sreenivasan, K. R., 1993, "The instability and breakdown of a round variable-density jet," *Journal of Fluid Mechanics* Vol.249, pp. 619-664.

Monkewitz, P. A., Bechert, D.W., Barsikow, B, and Lehmann, B., 1990, "Self-excited oscillation and mixing in a heated round jet," *Journal of Fluid Mechanics*, Vol. 213, pp. 611-639.

Monkewitz, P. A. and Sohn, K. D., 1988, "Absolute instability in hot jets," *AIAA. Journal*, Vol. 26, No.8, pp. 911-916, 1988.

Muramatsu, A., Gamba, M., and Clemens, T. N., 2008, "Side jets generated in a round helium gas jet," *Proceedings of 2nd International Conference on Jets, Wakes, and Separated Flows*.

Muramatsu, A., Saitoh, M. Kawabe, K and Kikuchi, T., 2015, "Side-Jet Formation in a Round Jet with Uniform Density," *Preprint of JSME Fluid Engineering Conference*, No. 0209, (in Japanese).

Muramatsu, A. and Hara, I., 2016, "Side-jets formation in a round jet with an external counter flow," *Preprint of JSME Fluid Engineering Conference*, No. 0210, (in Japanese).

Muramatsu, A. and Tanaka, K., 2021, "Flow structures in the initial region of a Round Jet with azimuthally deformed vortex rings utilizing a sound wave," Edited by Braza, M. et al., *Fluid-Structure-Sound Interaction and Control*, Springer, pp. 267-273.

Toyoda, K. Muramatsu, Y. and Hiramoto, R., 1999, "Visualization of the Vortical Structure of a Circular Jet Excited by Axial and Azimuthal Perturbations," *Journal of Visualization*, Vol. 2, No. 1, pp. 17-24.